PHYSICAL REVIEW B VOLUME 48, NUMBER 20 15 NOVEMBER 1993-II

Photon-emission scanning tunneling microscopy of silver films in ultrahigh vacuum: A spectroscopic method

A. W. McKinnon, M. E. Welland, and T. M. H. Wong
Department of Engineering, University of Cambridge, Cambridge CB2 1PZ, United Kingdom

J. K. Gimzewski
IBM Research Division, Zürich Research Laboratory, CH-8803 Rüschlikon, Switzerland
(Received 30 April 1993; revised manuscript received 26 July 1993)

We describe photon-emission scanning-tunneling-microscopy experiments on polycrystalline silver surfaces. By performing a method of simultaneous photon emission and tunneling spectroscopy measurements, we are able to show that the photon emission process and, in particular, the intergranular contrast in the photon maps depend upon interactions between individual grains in the silver film. Factors known to affect photon emission, such as grain shape and surface morphology, are shown to be inconsistent with the detailed structure of the photon maps. We observe that certain grains behave as isolated entities while others radiate in a more collective manner. This is indicative that for these materials the photon emission behavior is strongly affected by grain-boundary effects and we discuss a recent model which takes these into account.

INTRODUCTION

In this paper we describe the implementation of a spectroscopic form of photon-emission scanning tunneling microscope (PSTM) to determine the detailed characteristics of photon emission from condensed silver films in ultrahigh vacuum.

Since the initial reports in 1988,[1-3] the subject of photon emission from the STM has attracted considerable interest and it is instructive to review briefly the work in this area. The research falls into two broad areas depending on the type of sample studied; metals or semiconductors.

In the semiconductor field, photon emission studies started with investigation of light from Si(111),[1,4] however, the main research in this area has concentrated on III/V compounds with direct-band-gap materials such as GaAs,[5] $Ga_{1-x}Al_xAs$ (Refs. 6 and 7) heterostructures, and CdS.[8] Recently, such work has been extended to low-temperature STM on InP.[9]

For metal surfaces the physics of photon emission during STM is complex and requires new approaches both from the theoretical and experimental side, taking into account the nanometer proximity and electromagnetic coupling of the tip and the surface. Experiments carried out in this area are related to previous investigations by Lambe and McCarthy in 1976 (Ref. 10) of light emission from solid-state tunnel junctions fabricated in a metal-oxide-metal configuration. Controversies still exist regarding the mechanisms involved in light emission from such structures. With the STM, however, the freedom to vary experimental parameters on well characterized surfaces has permitted detailed investigations of the processes involved, and several theoretical models to predict the emission spectra have been proposed. Berndt, Gimzewski, and Johansson[11] presented a theoretical framework to establish the role of inelastic electron tunneling (IET) versus hot-electron injection as the excitation mechanism of localized plasmon modes based on the theory of Persson and Baratoff.[12] They have shown that the photon spectra can be modeled fairly well for Cu, Au, and to a lesser extent Ag surfaces. Here, as in all subsequent theories, IET was found to dominate.

The enhanced quantum efficiency noted on metals with this technique has, to date, been considered as resulting from the decay of localized tip-induced plasmon modes which emit directly.[13,14] However, the interpretation of the results from metals, in particular photon mapping, has been difficult. Experiments conducted in air suffer from problems of contamination and electrical breakdown [similar to metal-oxide-metal (MOM) junctions] at the voltages used (2 V), although Sivel *et al.*[15] have shown that on noble-metal surfaces photon mapping and spectroscopy are possible in air.

In this paper, we present a method to perform bias-dependent photon imaging with a STM, simultaneously with current mapping and barrier height mapping. This will facilitate a better understanding of the various geometrical and electronic factors that determine the local spectral efficiencies and afford more accurate comparison with the various theoretical models alluded to above. We have pursued this with the broader goal of developing techniques for obtaining local chemical information with the STM.

Normal operation of the STM is essentially controlled by elastic tunneling processes. Inelastic (dissipative) processes in the STM are usually swamped by the very much larger elastic tunneling current, and both the signal to background and signal to noise ratios are extremely unfavorable. However, as stated for metals, it is from this inelastic type of interaction that photon emission phenomena originate. Photon characteristics then contain

0163-1829/93/48(20)/15250(6)/$06.00

information which is closely linked to the chemical bonding and vibrational state of the species below the tip and should, ultimately, provide a spectroscopy which is more akin to conventional inelastic tunneling spectroscopy (IETS).

EXPERIMENTAL DETAILS

We have recently developed a mode of operation for the STM which allows photon mapping and spectroscopy for semiconductors and metals which we call photon imaging tunneling spectroscopy (PITS). The technique is an extension of the current imaging tunneling spectroscopy (CITS) scanning algorithm previously developed by Hamers, Tromp, and Demuth,[16] affording simultaneous analysis of the elastic and inelastic channels. The essence of the PITS technique is to perform photon spectroscopy at each image point by changing the tip bias and vertical displacements such that both spatial and energy variations of the photon signal can be determined at each point in the topographic image.

The data-acquisition algorithms required for the PITS experiments have been realized using a digital feedback and scanning control system based on an AT&T DSP32C digital signal processor (DSP) described elsewhere.[17]

In the CITS mode of operation,[16] the feedback loop is temporarily disabled maintaining a constant tip to surface separation at each picture point and the current level is measured at several selected voltages. In such an experiment, one acquires a topographic image together with several current images at different voltage biases. These data sets then contain spatially resolved local density of states (LDOS) information from the surface.

The PITS scanning algorithm measures inelastic tunneling effects as well as the elastic effects associated with CITS. At each picture point, emitted photons are counted with a photomultiplier tube and measured simultaneously with the current at each of a number of voltage biases and vertical displacements. The current-data LDOS information can be correlated with the integrated photon count (intensity), providing a map of the effective photon yield at different excitation voltages. The normalized photon yield gives information about local changes in emission probability which are not simply a result of local elastic conduction properties.

In addition, we can alter the vertical displacement of the tip (in 0.06-Å steps) to enhance the photon emission or to compensate for bias voltage levels lower than the equilibrium tunneling conditions maintaining signal-to-noise ratios.

If an AC modulation is applied to the tip-sample separation, phase-sensitive techniques may be used to obtain a map of local variation in the apparent barrier height simultaneously with the measurements of current level and photon intensity. This barrier height information may then be correlated with the current data and used to ascertain whether changes in local emission probability seen in the photon maps arise merely from simple changes in local conduction properties.

The photon emission experiments are carried out using a specially modified UHV compatible STM which has collection optics added to facilitate collection of photons emitted from the tip-sample tunneling junction. This microscope is routinely capable of providing atomic resolution on standard surfaces such as Si(111)-7×7 in UHV. Photon collection is achieved using an off-axis, ellipsoidal mirror, which is mounted such that the apex of the tip is at one of its focii. Thus, most of the light emitted from the tunneling region will be focused at the mirror's second focal point. This is arranged to be inside a photomultiplier tube situated external to the UHV chamber, through a kodial™ viewport. We estimate around 15% of the photons emitted in the energy range between 3 and 4.5 eV will be collected, taking all losses and collection efficiencies into account.

Silver films were cold deposited using a Knudsen cell *in situ* onto a Si(111)-7×7 surface and examined using the photon STM. The tunneling tips used in the experiments were made by electrochemically etching tungsten wire, and were cleaned first using a Kaufmann ion source and second by field emission in UHV before use in the STM.

RESULTS AND DISCUSSION

Silver films are viewed as ideal surfaces for photon emission experiments; very high quantum efficiencies are noted for them, arising from the low imaginary part of the silver dielectric function and a highly efficient plasmon mode at around 3 V which produces photons at experimentally acceptible energies. In order to measure significant photon yields, one often has to tunnel with high voltage biases and large tunneling currents:[1–3] these conditions are typically destructive to the tip and/or sample materials at room temperature and tend to cause unstable tunneling imaging behavior. In contrast, our technique allows us to control (i.e., acquire our topographic image) with acceptable tunneling parameters (a few volts tip bias, a few nA tunneling current) while momentarily varying the experiment conditions (voltage, current, or tip position) to those required to obtain good photon maps. Using the Ag on Si films described above, we first determine the optimum tunneling conditions for photon emission using a tungsten tip; we initially investigated how the photon intensity varies with the applied voltage at a constant tip-sample separation, and at constant voltage with varying separation.

Figure 1 shows a typical result from a constant separation I/V measurement recorded at normal tunneling conditions of -3 V and 2 nA. The photon emission has a turn on voltage of about -7 V, so we carried out PITS measurement at -7 and -8.5 V in order to obtain a good signal-to-noise ratio in the photon yield while controlling at -3 V, allowing stable tunneling.

In Fig. 2, we observe the behavior of the current and photon emission as the tip approaches the surface from the equilibrium tunneling conditions. The photon emission can clearly be seen to go through a maximum, which we attribute to "quenching" of the plasmon mode on decreasing tip to sample separation (this can be thought of in terms of impedence matching in a waveguide or, more interestingly, the possibility that a finite tunneling time is required to create the plasmon mode responsible for emission).

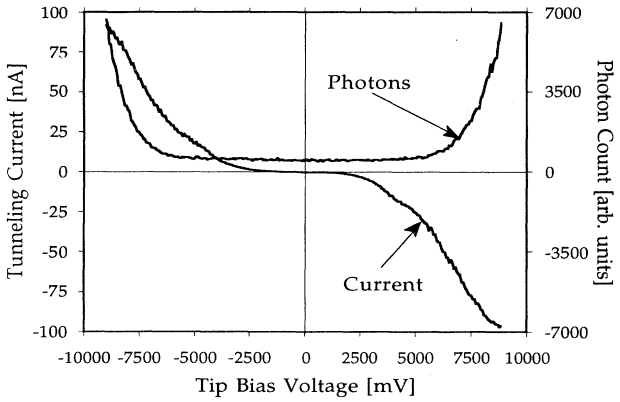

FIG. 1. A plot of the tunneling current and photon current versus applied tip-voltage bias, showing the typical bathtub response of the photon emission with voltage.

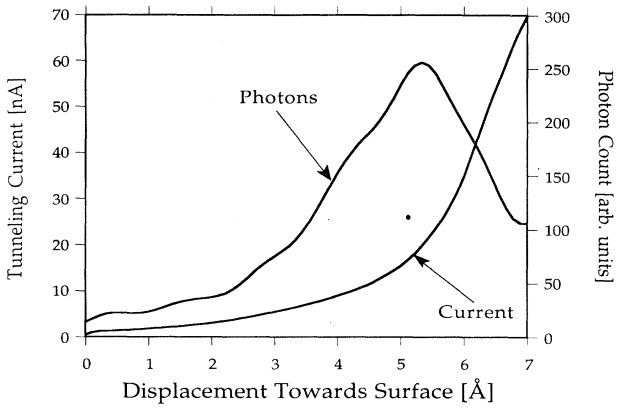

FIG. 2. A plot of the tunneling current and photon current versus tip to sample separation. Here the tip is moved towards the surface from the tunneling equilibrium conditions ($V=-3$ V, $I=1$ nA).

The silver deposited on the silicon forms a polycrystalline film with grains of 50→100 Å in diameter as shown in the STM constant current topographic image in Fig. 3(a). The current maps in Figs. 3(b) and 3(c) were obtained with the tip bias at −7 and −8.5 V, respectively, white regions representing high current. The current maps are consistent with the map of barrier height in Fig. 3(d), in that regions of high barrier height (bright) will give a low current level (dark) at constant separation. The current map at −8.5-V tip bias does not, however, show much image contrast because the current was too high, exceeding the dynamic range of the preamplifier. The photon map at −8.5 V [Fig. 3(f)] gives better image contrast than the photon map at −7 V [Fig. 3(e)]. This is probably because of the larger variations in current level at this voltage. It is important to note the pronounced contrast between grains both in the photon maps and in the current images. The entire set of images in Fig. 3 were acquired simultaneously in a time of 5 min.

Although not all the grains were individually resolved in the photon maps, the rapid change in signal level near

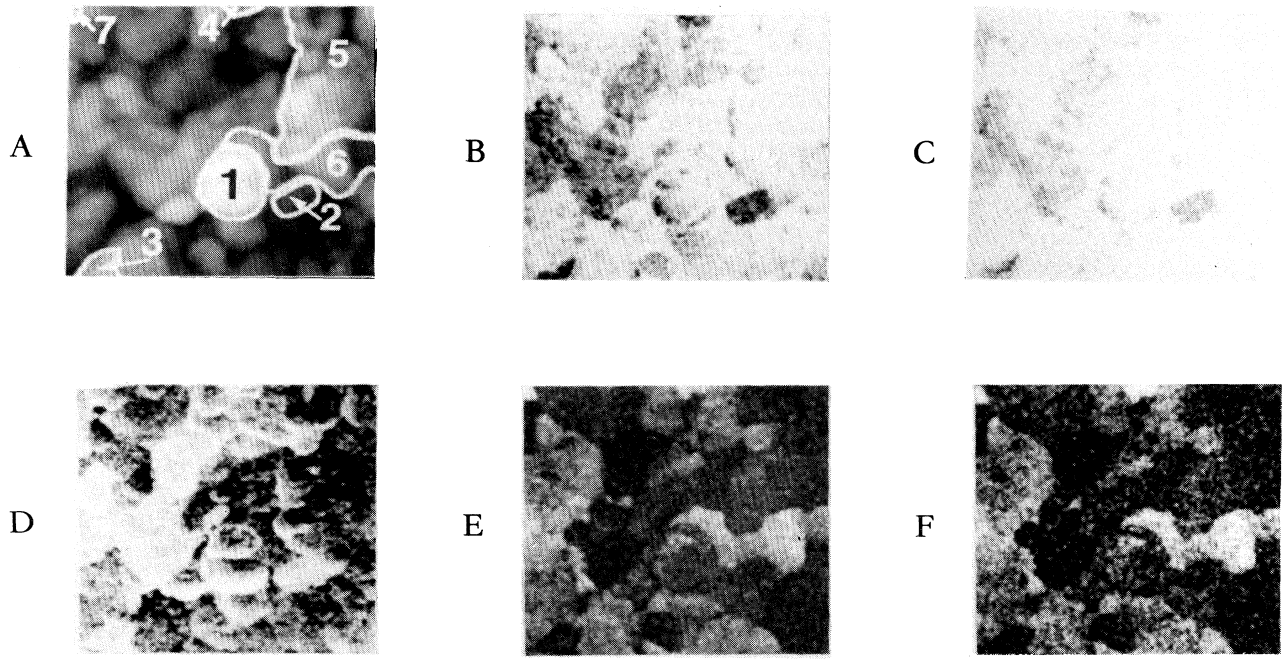

FIG. 3. A series of PITS data taken from a Ag surface. The images represent an area 450×450 Å^2 (×120 Å in the topography). (a) Topographic image taken with equilibrium tunneling conditions of $V=-3$ V, $I=1$ nA (the regions demarcated 1→7 are discussed later in the text). (b) Current map taken at the same equilibrium separation, but with $V=-7$ V. (c) Current map taken at the same equilibrium separation, but with $V=-8.5$ V. (d) Average barrier height map acquired simultaneously using the Z-modulation technique. (e) Photon map corresponding to current map (b). (f) Photon map corresponding to current map (c).

grain boundaries indicates near-atomic resolution (certainly less than 1 nm) in the photon signal. For a detailed analysis of the relative contrast levels in each of the images, it is useful to consider different regions in the images [as demarcated in the topographic image of Fig. 3(a)]. The most straightforward regions to analyze are those where the photon intensity scales with the current, such as region 6 in Fig. 3(a). This is the situation for a constant quantum efficiency in photon generation and corresponds to a constant ratio of elastic and inelastic tunneling. It is interesting to note that in Fig. 3 this type of simple relation between current and photon yield is the exception rather than the rule. Consider, for example, regions 4, 5, and 7. Region 5 exhibits a weak photon signal even though the current is high. Conversely, regions 4 and 7 show strong photon emission at low current levels. Careful inspection of the figure reveals that the latter regions are single grains in the topographic image. The simultaneously obtained topography and barrier height images [3(a) and 3(d)] give little insight into why there are some regions of the surface which give enhanced photon yield, even though the barrier height demonstrates contrast variations between grains.

Further complication is evidenced by the simultaneously acquired photon maps of Figs. 4(a)–4(c) taken at another region of the surface. These once again show the strong variation in photon emission from one grain to another but also indicate that there is a strong bias dependence of emission. For example, the grain *A* in Fig. 4(a) is only weakly emitting light at −6 V. There is a slight increase at −7 V [Fig. 4(b)] but at −8-V bias [Fig. 4(c)] it is strongly emitting. The light emitted from the majority of the grains increases with bias to a much lesser degree. These various observations indicate that there must be a contrast mechanism apart from topography and barrier height affecting the photon emission. We now consider this contrast in more detail.

The nature of the plasmon model between the tip and surface which is excited inelastically by tunneling electrons depends upon the dielectric functions of both the tip and surface as well as the tip-surface geometry.[12,18] If we assume that the tip shape and dielectric function remain constant during imaging, then it is only changes in surface properties which we need to consider. Based on a model of a spherical tip above a planar surface, Persson and Baratoff[12] demonstrated the dependence of photon yield on sphere diameter. As a crude approximation we can consider each grain of the film as a sphere with varying diameter. On this basis, we might expect variation in light emission from grain to grain simply due to the change in diameter. In the Persson and Baratoff calculation the dielectric function of the sphere remained constant, so that the change in light emission could be attributed solely to a geometric factor.

There are two problems associated with explaining the changes in light intensity from grain to grain based on the simple geometric variations described above. In the first case, although Persson and Baratoff predict a change in light emission with sphere size, the variation is much smaller than that found experimentally. For example, we find an intensity variation over the surface of nearly two orders of magnitude, while the grain size changes were only over a range from 2 to 5 nm. For a similar range in sphere size, the Persson and Baratoff model predicts changes of only a factor of 3. Second, and perhaps more importantly, the light intensity observed here has no obvious correlation with grain size. This is in agreement with the observations of Berndt, Grimzewski, and Johansson[11] and Sivel *et al.*[12] In the latter work, however, this change is attributed to changes in surface roughness. Although surface roughness is known to effect radiative decay of propagating surface plasmons, the only way that this can account for the observed intergranular contrast is if scattering takes place at the grain boundaries. Thus the plasmon mode would propagate over the grain surface until it was scattered at the grain boundary giving approximately constant photon contrast over the entire surface of any one grain during photon

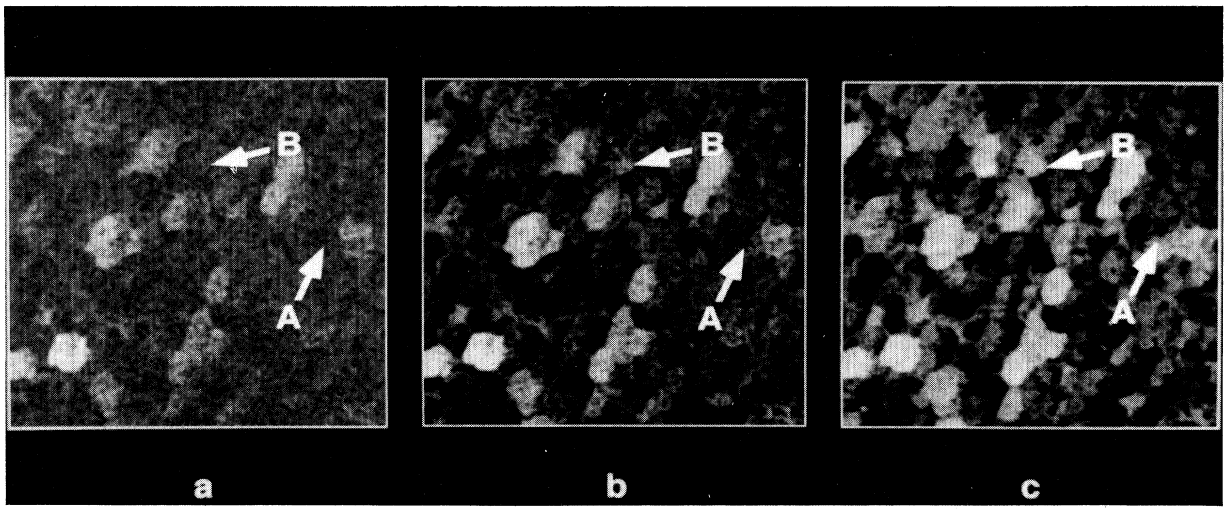

FIG. 4. Photon maps corresponding to an area 1280×1280 Å^2 showing the emitted photons at a voltage of −6 V (a), −7 V (b), and −8 V (c). The lighter regions correspond to more photon being emitted, with a maximum count of 20 000 counts/sec at the detector. Strong intergranular contrast is apparent in the photon maps.

imaging. This could only be true if the plasmon mode induced at the tip coupled effectively into a surface traveling mode which was then scattered. Both the coupling process itself and the relative probabilities of exciting localized and traveling modes are at present the subject of some controversy and hence no firm conclusions can be drawn as to their role in the granular contrast observed here. It should be remembered that the growth mechanism of Ag polycrystalline films is columnar and the aspect ratio of individual crystallites is quite variable. Thus, the plasmon modes set up in the grains will depend on this aspect ratio, since the coupling depends on the relative orientation of the long axis of the grain with respect to the tip shape orientation. To date this aspect ratio has not been included in any of the spherical models. However, we do not consider this as being a dominant effect here.

From the preceding arguments, we see that geometrical factors are not the main parameters governing the observed granular contrast. We must, therefore, consider the possibility of the observed contrast resulting from changes in the local dielectric properties. The plasmon mode responsible for photon emission is dependent on the dielectric functions of both surface and the tip, however, the tip is assumed to be stable and thus we need only consider changes in the silver dielectric properties as contributing to the contrast. It is likely that there are small changes in the surface dielectric function dependent upon the crystal orientation of the grain. This is analogous to the demonstration by Smolyaninov, Khailkin, and Edelman[19] of the dependence of photon emission on a number of different material tip-surface combinations; here they essentially saw the effect of changing the dielectric function, although they did not consider the geometrical factor which would have varied from measurement to measurement, their observed variations were less than we observe between grains of ostensibly the same material.

If we consider our results again we see that the delineation in contrast is predominantly determined by the position of grain boundaries in the material. It seems that the cooperative behavior of particular regions are determined by the below surface coupling of different regions at grain boundaries.

Recently, such a model has been considered by Baratoff, where he explains the observed intergranular contrast in the photon maps based on how well the grains "couple" electronically between themselves and to the bulk material.[20] In this case, each grain is considered to have an associated time constant which is dependent on how well the grain can sink or source charge, to or from the bulk. Thus, we could have charging of grains which will dynamically modify the potential seen by the tunneling electrons and the plasmon interactions over particular grains, hence modifying the photon emission probabilities. The origin of such a time constant for grains in a well-connected, granular-structure film is not obvious, although they could be related to the relative crystallographic orientation of the grains which exhibit a predominant (111) surface texture. These effects, though, are related to the phenomena discussed by Kirtley, Washburn, and Brady,[21] in their work using the STM to directly measure potential differences across grain boundaries in the presence of a lateral current flow. In our case, the phenomenon can clearly be seen if we compare equivalent parts of the topographic and photon map images in Fig. 4. In region 6, a collection of grains, as apparent in the topographic image, are seen to emit fairly uniformly in the photon maps. Here we can see that the transition to less-emitting regions does not just follow simple isolated grain boundaries, but rather seems to involve some more complex connected structures. Thus, the emission from a particular grain is dominated by the grain boundary surrounding it. Baratoff has found that the photon emission from a well "grounded" sphere is significantly lower than that from an equivalent sphere in which a time constant has been added between it and a hypothetical counter electrode.

Finally, it is possible to make a crude estimate of the degree of localization of the tip-surface plasmon mode, and hence the spatial resolution in photon maps, using the model similar to that of Rendell and Scalapino[18] of a sphere above a plane. They show that the mode is localized over a distance set by the geometric mean of the particle radius and the particle film separation. Taking a particle radius of 5 nm (a typical grain size observed) and a tunnel gap of 1 nm gives a localization of ~ 2 nm. This then sets a lower limit to the spatial resolution obtained in the photon maps. For smaller grains and/or tip radii this figure would decrease to ~ 1.5 nm. This will be complicated by scattering effects at grain boundaries which may lead to enhanced resolution.

CONCLUSIONS

We have developed a scanning technique to perform spatially resolved photon emission and tunneling spectroscopy measurements simultaneously. Silver deposited on silicon was used as the test sample, and we found that near-atomic resolution can be obtained in the photon maps. The observed intergranular contrast is found to be inconsistent with existing models which consider just geometric and dielectric propeties of the system. A more accurate explanation would have to include the effects of grain boundaries and steps have been made in constructing such models.

When allied to optical spectrum analysis the technique promises to give a complete spectroscopic picture for tunneling interactions, in that we will be able to obtain spatial and energy resolved elastic and inelastic data for different materials. The ultimate goals of the technique are to provide a means of analyzing local chemical and dielectric properties in the tunneling microscope (which will of course only be obtainable from the inelastic interaction data) and to allow investigations on fundamentally important materials (such as interactions on isolated, excited molecules).

ACKNOWLEDGMENTS

We would like to acknowledge Dr. M. E. Taylor, A. Downes, and R. Stephenson for many valuable discussions.

[1]J. K. Gimzewski, B. Reihl, J. H. Coombs, and R. R. Schlittler, Z. Phys. B **72**, 497 (1988).
[2]J. H. Coombs, J. K. Gimzewski, B. Reihl, J. K. Sass, and R. R. Schlittler, J. Microsc. **152**, 325 (1988).
[3]J. K. Gimzewski, J. K. Sass, R. R. Schlittler, and J. Schott, Europhys. Lett. **8**, 435 (1989).
[4]S. Ushioda, Solid State Commun. **84**, 173 (1992).
[5]S. F. Alvarado and P. Renaud, Phys. Rev. Lett. **68**, 1387 (1992).
[6]D. L. Abraham, A. Veider, Ch. Schönenberger, H. P. Meier, D. J. Arent, and S. F. Alverado, Appl. Phys. Lett. **56**, 1564 (1990).
[7]P. Renaud and S. F. Alvarado, Phys. Rev. B **44**, 6340 (1991).
[8]R. Berndt and J. K. Gimzewski, Phys. Rev. B **45**, 14 095 (1991).
[9]L. Montelius, M. E. Pistol, and L. Samuelson, Ultramicrosc. **42-44**, 210 (1992).
[10]J. Lambe and S. L. McCarthy, Phys. Rev. Lett. **37**, 923 (1976).
[11]R. Berndt, J. K. Gimzewski, and P. Johansson, Phys. Rev. Lett. **67**, 3796 (1991).
[12]B. N. J. Persson and A. Baratoff, Phys. Rev. Lett. **68**, 3224 (1992).
[13]P. Johansson, R. Monreal, and P. Apell, Phys. Rev. B **42**, 9210 (1990).
[14]Y. Uehara, Y. Kimura, S. Ushioda, and K. Takeuchi, Jpn. J. Appl. Phys. **31**, 2465 (1992).
[15]V. Sivel, R. Coratger, F. Ajustron, and J. Beauvillain, Phys. Rev. B **45**, 8634 (1992).
[16]R. J. Hamers, R. M. Tromp, and J. E. Demuth, Phys. Rev. B **34**, 5343 (1986).
[17]T. M. H. Wong and M. E. Welland, Meas. Sci. Technol. **4**, 270 (1993).
[18]R. W. Rendell and D. J. Scalapino, Phys. Rev. Lett. **41**, 1746 (1978).
[19]I. I. Smolyaninov, M. S. Khaikin, and V. S. Edelman, Phys. Lett. A **149**, 410 (1990).
[20]A. Baratoff (private communication).
[21]J. R. Kirtley, S. Washburn, and M. J. Brady, Phys. Rev. Lett. **60**, 1456 (1988).

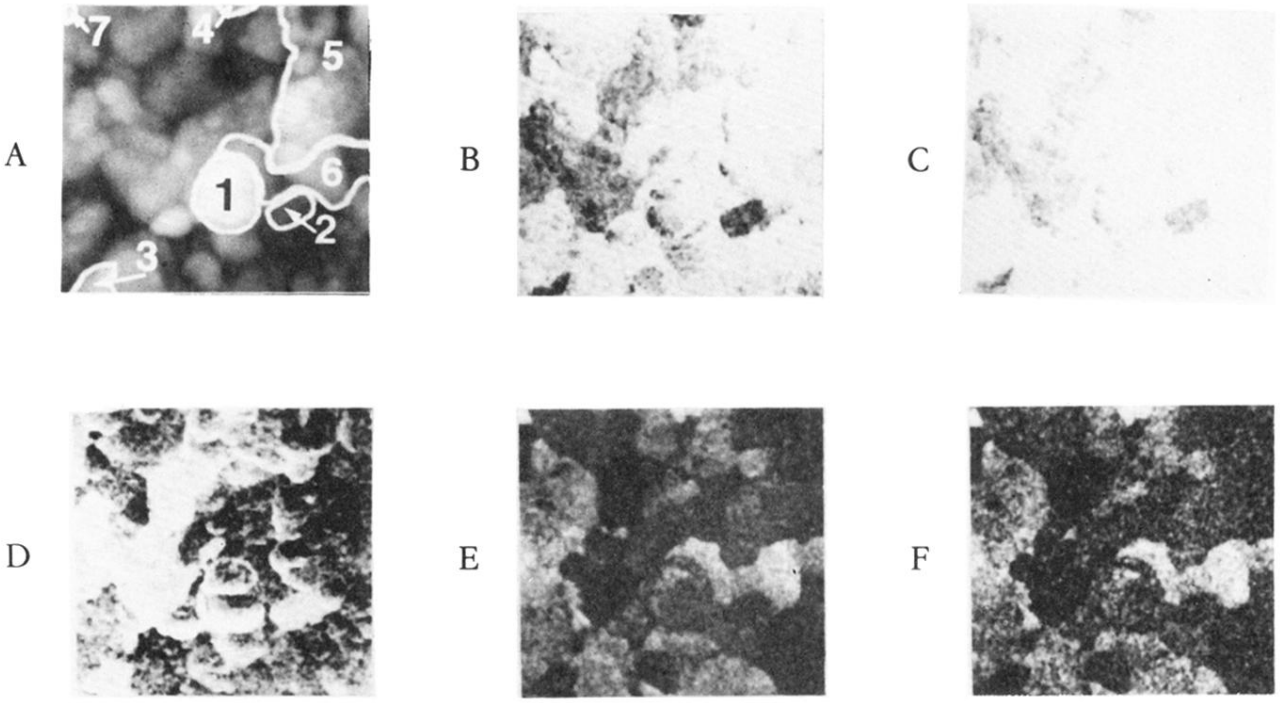

FIG. 3. A series of PITS data taken from a Ag surface. The images represent an area 450×450 Å^2 (×120 Å in the topography). (a) Topographic image taken with equilibrium tunneling conditions of $V=-3$ V, $I=1$ nA (the regions demarcated 1→7 are discussed later in the text). (b) Current map taken at the same equilibrium separation, but with $V=-7$ V. (c) Current map taken at the same equilibrium separation, but with $V=-8.5$ V. (d) Average barrier height map acquired simultaneously using the Z-modulation technique. (e) Photon map corresponding to current map (b). (f) Photon map corresponding to current map (c).

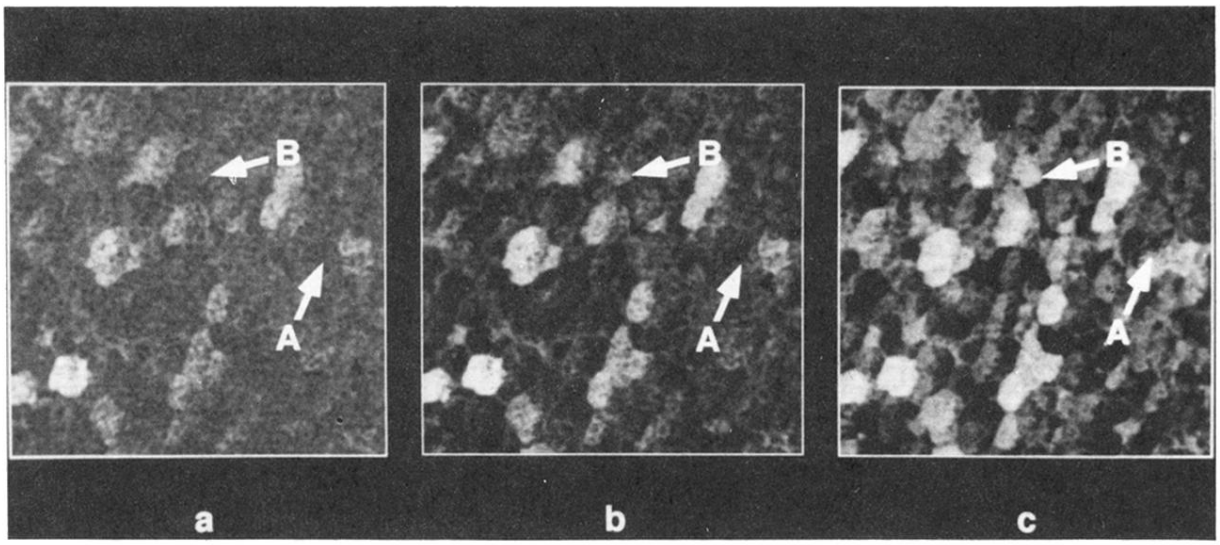

FIG. 4. Photon maps corresponding to an area 1280×1280 Å^2 showing the emitted photons at a voltage of -6 V (a), -7 V (b), and -8 V (c). The lighter regions correspond to more photon being emitted, with a maximum count of 20 000 counts/sec at the detector. Strong intergranular contrast is apparent in the photon maps.